Optimization of a pixellated CdZnTe/CdTe detector for a multi-modality imaging system

Pedro Guerra *IEEE Graduate Student Member,* Dimitra G. Darambara *IEEE Member,*
Dimitris Visvikis *IEEE Senior Member* and Andres Santos *IEEE Senior Member*

Abstract— **The operation of any semiconductor detector depends on the charges movement created in the material after energy deposition. The charge in the bulk semiconductor induces image charges on the metal electrodes and therefore the charge movement towards the electrodes induces a current in the electrodes and external circuit. The details of how quickly and how far the bulk charge travels depend on the material parameters of mobility (μ) and lifetime (τ), as well as the operating electric fields (E). The amount of image charge present at any instant of time (for a given amount of bulk charge) depends on the position of the bulk charge and the weighting potential of the electrode, which depends on the device structure and biasing. The design of the detector can therefore have a significant impact on its spectral performance.**

I. Introduction

THE INTEREST on room temperature semiconductor detectors with high atomic numbers, like CdTe/CdZnTe, for gamma ray imaging in Nuclear Medicine (NM) applications has been steadily increasing in the last decade, supported by recent advances in crystal growth. Both materials have numerous advantages as radiation detectors, but one of their most important drawbacks is their poor hole transport. In order to reduce this handicap, different structures such as strips [2] or pixels [3], have been proposed in order to enhance the signal induced by electrons moving close to the anode and minimize the contribution of hole transport.

The primary reason for investigating solid-state detectors for NM is the potential for their improved energy resolution over scintillators, in order to provide superior Compton scatter rejection; for example at 140 keV a value of 3-4 keV (2-3%) FWHM would reduce the scatter component of the image reconstruction error to a level below that of the photon statistics when using 99mTc [4], however a more relaxed constrain of 5% FWHM resolution will be imposed, which is still far bellow that achievable with scintillators. Moreover, these energy resolution figures enable multi-isotope imaging [5], providing the potential to revolutionize functional imaging [6].

This work is aimed at determining the optimum configuration and material in the energy range that goes from x-rays (10-40 keV) to PET imaging (511 keV) of a pixellated detector. It is known the optimum configuration to maximize the small pixel effect may differ depending on the charge carriers transport characteristics and therefore accurate simulation is required in order to find the best setup.

Moreover, in the case of a multimodality imaging systems, additional tradeoffs have to be taken into consideration in order to provide the best trade-off within a wide energy spectrum and possible competing imaging modality requirements.

Optimization is based on an ad-hoc 3D simulator that extends the approach described in [7] by incorporating a simplified Montecarlo (MC) simulator that computes gamma energy deposition in the material and integrating a more complete noise model to estimate the contribution of the different sources of noise for the different scenarios under consideration.

The present work is organized in three sections, firstly the structure of the simulator is described, secondly the scenarios simulated will be presented and finally the conclusions are given. Results focus on estimating performance parameters such as energy resolution, efficiency or intrinsic spatial resolution for different detector dimensions and transport properties.

II. Material and Methods

A. "Pseudo-Monte Carlo" simulator

The implemented simulator, which extends the pseudo Montecarlo (MC) approach described by [7], consists on the following seven steps:

1. *Photon interaction*: At the gamma energies under consideration, there is no pair production and it may be assumed that inelastic scattering is the dominant process in the upper range of interest while photoelectric absorption plays a major role at lower energies. These facts enormously simplify the physics of the radiation-matter interaction.

Manuscript received November 15, 2007. This work has been supported by Spanish Ministry of Education, through the FPU Grant program, by the regional research program PDIMM (CCG06-UPM/BIO-0502) and by the EU-funded EMIL network (LSHC-CT-2004-503569).

P. Guerra and A. Santos are with the Universidad Politecnica de Madrid, E-28040, Spain, (telephone: +34-915495700-4242, e-mail: pguerra ,andres @die.upm.es).

D.Visvikis is with the Laboratoire de Traitement d'Information Medicale (LaTIM), 5 avenue Foch, Brest ,F-29609, France (telephone :+33-0298018114, e-mail: dimitris@univ-brest.fr)

D. Darambara is with the Royal Marsden NHS Foundation Trust / Institute of Cancer Research, Fulham Road, London SW3 6JJ, UK, (telephone: +44-(0)207-808-2502, email: Dimitra.Darambara@icr.ac.uk)

The simplified MC simulator provides radiation-matter interactions, consisting on a list of Compton depositions and possibly a final photoelectric deposition for every gamma. In case of Compton interactions, the photon is scattered in a direction given by the azimuthal angle φ, the polar angle θ, where the former is uniformly distributed between 0 and 2π while θ follows the Klein-Nishina probability distribution.

CdTe and CdZnTe cross section values between 10 keV and 1 MeV are taken from photon cross section database of the National Institute of Standards and Technology [8].

Energy depositions are considered punctual and therefore subsequent x-ray and/or Auger electron emissions are neglected for the time being in this simplified model. .. However, this effect may be of importance in the case of very small pixels, as discussed in [9].

2. *Hole-electron pairs generation*: Each gamma interaction produces a variable number *N* of electron-hole pairs. The actual number of carriers is function of the deposited energy and material properties and follows the Poisson statistics, which for large numbers converges to a Gaussian distribution.

3. *Charge Trapping*: Each charge carrier either reaches its electrode or is trapped at some point along the way. The ultimate fate of the carrier depends on the material transport properties, detector dimensions and biasing voltage. The lifetime $t_{h,e}$ of each charge carriers is exponentially distributed an depends on the charge carrier average lifetime.

4. *Charge Diffusion*: During its lifetime, each charge carrier diffuses laterally in the x,y plane while travelling at constant speed in the z direction driven by the uniform electric field. Considering a uniform electric field is certainly the weakest approximation of this work, however greatly simplifies the modelling enabling the decoupling between the x,y Brownian motion and charge transport in z.

The diffusion distance dr along the radial axis is function of the diffusion constant as follows,

$$d^{r}_{h,e} \sim G\left(0,\sigma^{2}_{h,e}\right)\begin{cases}\sigma^{2}_{h,e} = 2\cdot D_{h,e}\cdot t_{h,e}\\ D_{h,e} = \dfrac{kT}{q}\mu_{h,e}\end{cases} \qquad (1)$$

Where *k* is the Boltzmann constant, *T* is the temperature and *q* is the electron charge.

5. *Electrode Charge Induction*: Each charge carrier induces a charge on the readout anode/cathode which is estimated based on Ramo's theorem. This theorem states that the induced charge *Q* may be computed as the difference between the weighting potential as seen by the anode φ_a and the cathode φ_c of the electron/hole pair at its final points. The actual values for the weighting potentials are computed based on the 3D approximation provided in[10]

6. *Hit Fusion*: The energy readout by the system is the sum of all the hits belonging to the same gamma.

7. *Noise*: Two main noise sources are considered: the detector, mainly due to the leakage current, and the electronics, which contribute mainly through the low-noise preamplifier and feedback resistors. These two noise sources contribute to the total Noise Equivalent Charge (NEC) as the sum of different white and/or pink parallel and series contributions [11].

$$NEC^{2} = NEC^{2}_{PREAMP} + NEC^{2}_{DETECTOR} \qquad (2)$$

At the preamplifier, we shall consider the loading capacitances, including the detector C_{ext}, the preamplifier input capacitance C_{in}, the shaping constant of the filters τ_{shape}, the transconductance of the preamplifier transistor gm , the feedback resistor value Rp, the preamplifier bias current I_{dc} and other coloured noise contributions, which are proportional to the load and parasitic capacitances.

$$NEC^{2}_{PREAMP} = \begin{array}{l}\dfrac{F_{s}}{\tau_{shape}}\cdot\dfrac{4KT}{q^{2}}\dfrac{2}{3g_{m}}\left(C_{in}+C_{d}\right)^{2}+\ldots\\ F_{p}\tau_{shape}\cdot\left(\dfrac{4KT}{q^{2}}\dfrac{1}{R_{p}}+\dfrac{2I_{dc}}{q}\right)+NEC^{2}_{1/f}\end{array} \qquad (3)$$

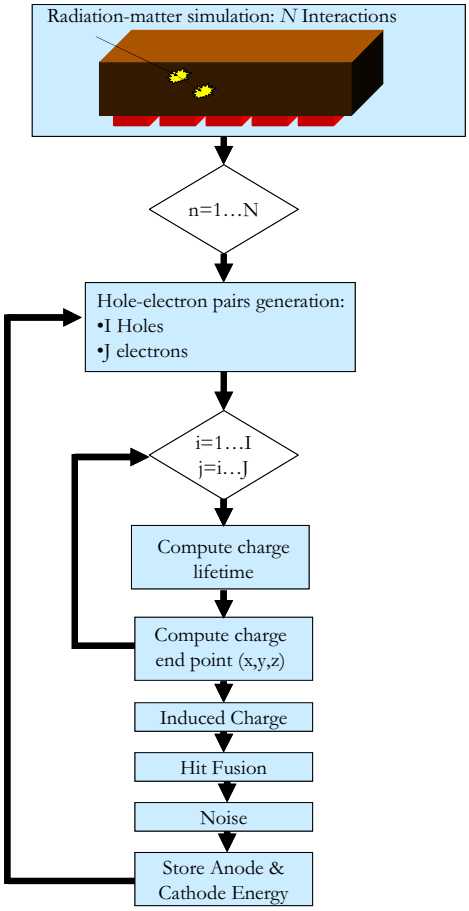

Fig. 1: Integrated simulator flow chart.

Table 1: Main material properties [1]

	$Cd_{0.9}Zn_{0.1}Te$	CdTe
Density (g/cm^3)	5.78	5.85
Resistivity (Ω•cm)	$3x10^{10}$	$1.5x10^{10}$
Electron lifetime (s)	$3x10^{-6}$	$3x10^{-6}$
Hole lifetime (s)	10^{-6}	$2x10^{-6}$
Dielectric Constant	10.9	11
Pair creation energy (eV)	4.64	4.43
Electron mobility (cm^2/Vs)	1000	1100
Hole mobility (cm^2/Vs)	50–80	100
Fano Factor	0.2	0.14

Where F_s, F_p are the form factor for the readout filters, q is the electron charge, K is the Boltzmann constant and T is the temperature.

This simulator have been developed with Matlab 7.1 (The Mathworks, Natick, MA, USA) and the computation phases are arranges following the flow chart shown in Fig. 1.

III. Results

Results are divided into two phases. Firstly, the noise model given by equation 6 is parameterized according with the electronics descriptions provided in [12], which are summarized in table 2. The $NEC_{1/f}$ proportionality factor is computed to account for the fact that in the ASIC pre-amplifier noise is dominated by flicker noise. After the inclusion of this 1/f noise factor $K_{1/f}$, the model predicts a NEC linear increase with the external capacitance C_{ext} of 85e+11 e/pF with τ=10 us, as shown in Fig. 2, value that very well matches the measured electronic noise of 56e+11.6 e/pF and the experimental base level noise of 85 eV.

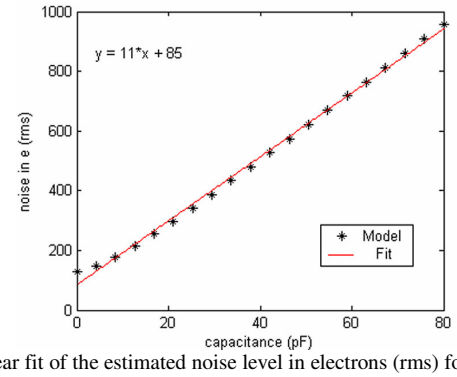

Fig. 2: Linear fit of the estimated noise level in electrons (rms) for τ=10us.

The NEC values shown in Fig. 3 have been computed for shaping constants between 100 ns a 50 us, external capacitances of 2pF,5pF ans 10 pF and a bulk current of 250 pA/pixel, which is consistent with data published in [13]. For the presented scenario, NEC is estimated to be lower than e (rms).

Table 2: Electronics Settings

PreAmp Transconductance Gm (mS)	3.5
CSA Feedback Resistor Rfp (GΩ)	1
CSA Input Capacitance Cint (pF)	2.5
External Capacitance Cext (pF)	5
First Order CRRC shaping FP=FS	$e^2/8$=0.92
Shaping Time τ (μs)	6
ENC e (RMS)	<250
Dielectric capacitance (pF)	1
Dielectric loss factor	10^{-4}

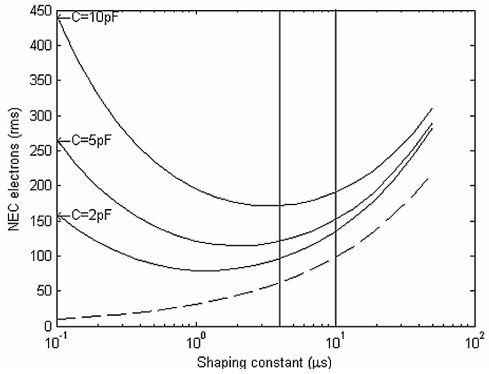

Fig. 3: Estimated NEC for variable shaping constants and detector's capacitance of 2pF,5pF and 10 pF. Detector's shot noise is plotted in dashed line to provide a reference.

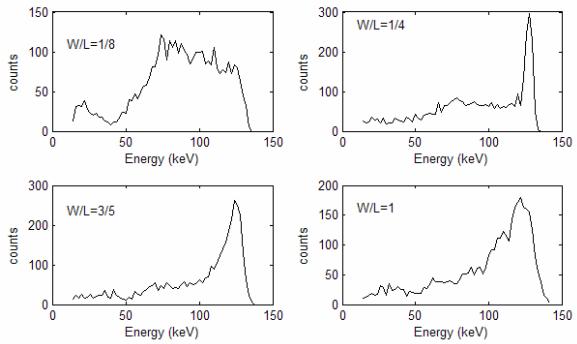

Fig. 4: Estimated CdTe pixel spectrum at 140keV for a 4 mm thick detector, nominal transport properties and 400 V biasing.

Pixel performance is simulated for CdTe and CdZnTe, with the material properties summarised in Table 1. As an example Fig. 4 shows the simulated results for CdTe with different aspect ratios and 140 keV incident gammas, where for the given transport properties the best resolution is obtained around W/L=0.25, as it is shown in Fig. 5.

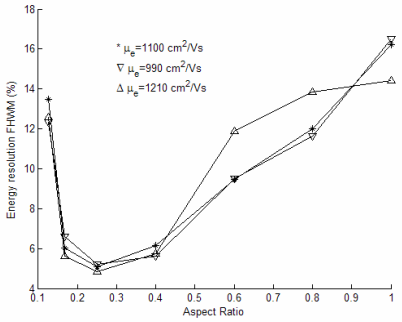

Fig. 5: Estimated energy resolution FHWM with CdTe at 140 keV with W/L between 0.1 and 1 and nominal (*) transport properties as well as 10% below (Δ) and 10% above (∇).

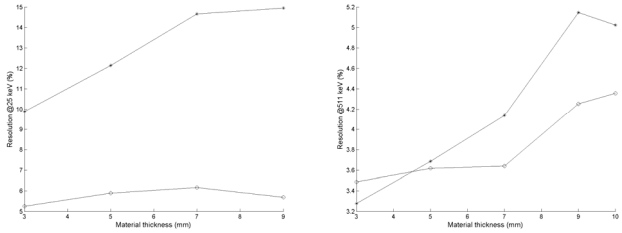

Fig. 6: Simulated resolution at 25 keV and 511 keV

Resolution, shown in Fig. 6, is computed as the FWHM around the photopeak. It is shown that, for the considered material properties in Table 1, CdZnTe (o) provides higher energy resolution than CdTe (*) at all energies and thicknesses. These performance figures can still be improved with biparametric techniques [14] aimed at compensating the lower charge induction efficiency close to the anodes. Figure shows that 6% restriction on energy resolution rules out the use of CdTe at room temperature, due to the excessive noise because of its lower bulk resistivity. However, at high energies CdTe performs slightly better than CdZnTe.

IV. Conclusions and Future Work

This work has set up the simulation framework for the optimization of a pixellated room temperature detector for a multimodality imaging system, with a special focus on the accurate modelling of the noise sources, whose parameters are adjusted to reproduce experimental measurements with an existing readout ASIC provided by other authors.

Current results show the importance of material properties and detector dimensions for an optimum energy resolution. The resulting model will be used to estimate pixel energy spectrum for CdTe and CdZnTe detectors with resistive readout at 4 energies with different thicknesses, pixel ratios and transport mobility properties. The goal of these simulations will be to determine the optimum detector setup for a CZT/CdTe-based multimodality scanner.

References

[1] eV Products, "Material Properties," in *http://www.evproducts.com/material_prop.pdf*, 2006.

[2] L. A. Hamel, *et al.*, "Signal generation in CdZnTe strip detectors", *IEEE Transactions on Nuclear Science*, vol. 43, pp. 1422 - 1426, 1996.

[3] P. R. Bennett, *et al.*, "High efficiency pixellated CdTe detector ", *Nuclear Instruments and Methods in Physics Research Section A*, vol. 392, pp. 260-263, 1997.

[4] P. R. Bennett, *et al.*, "Evaluation of CdTe for use in a prototype emission/transmission CT imaging system", *IEEE Transactions on Nuclear Science*, vol. 43, pp. 2225-2229, 1996.

[5] L. Verger, *et al.*, "New perspectives in gamma-ray imaging with CdZnTe/CdTe," at *IEEE Nuclear Science Symposium Conference Record*, vol. 4, pp. 2313 - 2319, 2004.

[6] J. Patton, *et al.*, "D-SPECT: A new solid state camera for high speed molecular imaging", *Journal of Nuclear Medicine: Meeting Abstracts*, vol. 47, pp. 189, 2006.

[7] A. Zumbiehl, *et al.*, "Modelling and 3D optimisation of CdTe pixels detector array geometry - Extension to small pixels", *Nuclear Instruments and Methods in Physics Research Section A*, vol. 469, pp. 227-239, 2001.

[8] M. J. Berger, *et al.*, "XCOM: Photon Cross Sections Database. NIST Standard Reference Database 8 (XGAM)," vol. 2007. http://physics.nist.gov/PhysRefData/Xcom/Text/XCOM.html, 1998.

[9] K. Iniewski, *et al.*, "Modeling Charge-Sharing Effects in Pixellated CZT Detectors," at *IEEE Nuclear Science Symposium and Medical Imaging Conference*, Honolulu, USA), 2007.

[10] A. Castoldi, *et al.*, "Three-dimensional analytical solution of the Laplace equation suitable for semiconductor detector design", *IEEE Transactions on Nuclear Science*, vol. 43, pp. 256 - 265, 1996.

[11] V. Radeka, "Low-Noise Techniques in Detectors", *Annual Review of Nuclear and Particle Science*, vol. 38, pp. 217-277, 1988.

[12] D. M. Pettersen, *et al.*, "A readout ASIC for SPECT", *IEEE Transactions on Nuclear Science*, vol. 52, pp. 764 - 771, 2005.

[13] B. P. F. Dirks, *et al.*, "Leakage current measurements on pixelated CdZnTe detectors", *Nuclear Instruments and Methods in Physics Research Section A*, vol. 567, pp. 145-149, 2006.

[14] L. Verger, *et al.*, "Performance and perspectives of a CdZnTe-based gamma camera for medical imaging", *IEEE Transactions on Nuclear Science*, vol. 51, pp. 3111- 3117, 2004.